

Chemical tailoring of sodium content for optimization of interfacial band bending and alignment in flexible kesterite solar cells

Ha Kyung Park^a, Yunae Cho^a, Juran Kim^a, Gee Yeong Kim^b, Woo-Lim Jeong^{c,d},
Kyung-Pil Kim^{c,d}, Dong-Seon Lee^{c,d,**}, William Jo^{a,*}

^a Department of Physics and New and Renewable Energy Research Center, Ewha Womans University, Seoul, 03760, Republic of Korea

^b Advanced Photovoltaics Research Center, National Agenda Research Division, Korea Institute of Science and Technology (KIST), Seoul, 02792, Republic of Korea

^c School of Electrical Engineering and Computer Science, Gwangju Institute of Science and Technology (GIST), Gwangju, 61005, Republic of Korea

^d Research Institute for Solar and Sustainable Energies, Gwangju, 61005, Republic of Korea

ARTICLE INFO

Keywords:

Flexible CZTSSe
Na-passivated grain boundaries
Band bending
Photo-assisted Kelvin probe force microscopy
Photogenerated carrier transport

ABSTRACT

In this study, highly efficient and flexible Na-doped kesterite $\text{Cu}_2\text{ZnSn}(\text{S,Se})_4$ (CZTSSe) thin-film solar cells with an efficiency of over 8% were developed. A CZTSSe thin film was deposited on a flexible Mo foil using metal precursors with varying thickness of the NaF layers on the CZTSSe thin film. The sample maintained 92.2% of its performance after 1000 bending cycles with a bending radius of 12 mm. To investigate defect passivation effect of Na doping through the electrical properties of Na-passivated grain boundaries (GBs), the cells were examined by scanning probe microscopy. Downward band bending was observed at GBs in the Na-sufficient CZTSSe absorber layers; that is, Na enhanced the potential barrier at the CZTSSe GBs in the solar cells and the separation of carriers. The carrier separation increased under illuminated condition. Moreover, the surface photovoltage (SPV) of the cells was measured at laser wavelengths of 405, 532, and 640 nm using photo-assisted Kelvin probe force microscopy to investigate the photogenerated carrier transport in Na-passivated CZTSSe solar cells. The Na content strongly affected the photo-induced changes in the carrier behavior. A cell with a sufficiently Na-doped CZTSSe absorber layer exhibited a large SPV with a maximum value of 46 meV under illumination, whereas Na-deficient samples showed a lower SPV, indicating that Na passivates defects that act as recombination sites. A photo-induced defect passivation effect was observed in a cell with optimal Na content under 405 nm wavelength illuminated condition, which resulted in charge accumulation at the absorber surface.

1. Introduction

Kesterite ($\text{Cu}_2\text{ZnSn}(\text{S,Se})_4$, CZTSSe) is a promising photovoltaic absorber material because of its suitable physical properties such as a direct energy band gap that is tunable from 1 to 1.5 eV by adjusting the ratio of S to Se, and high absorption coefficient [1–3]. However, the highest power conversion efficiency (PCE) achieved by CZTSSe thin-film solar cells to date is 12.6%, whereas that of $\text{Cu}(\text{In,Ga})\text{Se}_2$ (CIGS) thin-film solar cells is 23.35% with a CdS buffer layer and 22.9% without the CdS buffer layer [4–6]. However, despite the high efficiency of the CIGS thin-film solar cells, their use of In and Ga limit their wide application. By replacing In and Ga in CIGS with Zn and Sn, which are

relatively inexpensive and abundant, i.e., using CZTSSe instead of CIGS, the manufacturing cost of thin-film solar cells can be lowered [7,8]. Furthermore, attempts have been made to replace the rigid substrates of solar cells with thin, lightweight flexible substrates for wide application. For example, a CIGS solar cell on a flexible polyimide (PI) substrate with a PCE exceeding 20% has been reported [9].

Flexible glass, stainless-steel, PI, and metal foils, such as Mo, Ti, and Al foils, are considered as promising substrate materials for use in flexible kesterite thin-film solar cells. Among them, the metal foils possess high conductivity, which can lead to the development of a low-cost, roll-to-roll production. In particular, the Mo foil has attracted attention owing to the lack of metallic impurities and its compatible

* Corresponding author. Department of Physics, Ewha Womans University, 52 Ewhayeodae-gil, Seodaemun-gu, Seoul, 03760, Republic of Korea.

** Corresponding author. School of Electrical Engineering and Computer Science, Gwangju Institute of Science and Technology (GIST), 123 Cheomdan-gwagiro, Buk-gu, Gwangju, 61005, Republic of Korea

E-mail addresses: hakyungpark@ewhain.net (H.K. Park), yachop@ewha.ac.kr (Y. Cho), jurankim@ewhain.net (J. Kim), gykim@kist.re.kr (G.Y. Kim), wljeong@gm.gist.ac.kr (W.-L. Jeong), kyungpil@gist.ac.kr (K.-P. Kim), dslee66@gist.ac.kr (D.-S. Lee), wmjo@ewha.ac.kr (W. Jo).

<https://doi.org/10.1016/j.solmat.2021.111243>

Received 11 December 2020; Received in revised form 7 June 2021; Accepted 13 June 2021

Available online 24 June 2021

0927-0248/© 2021 Elsevier B.V. All rights reserved.

thermal expansion, $5.2 \times 10^{-6} \text{ K}^{-1}$ [10–12]. The CZTSSe thin-film solar cells using the flexible glass and the Ti foil substrates have achieved PCEs of 6.90% and 2.00%, respectively [13,14]. Since Zhang et al. [15] first reported a PCE of 3.82% for a $\text{Cu}_2\text{ZnSnS}_4$ (CZTS) thin-film solar cell on the Mo foil, there have been an increasing interest in utilizing the Mo foil as a flexible substrate. The PCEs of the CZTSSe thin-film solar cells using the Mo foil have reached 6.78% for those fabricated by solution-based processes and 8.00% for those produced by sputtering [16,17]. Considering that the highest PCE of a CZTSSe thin-film solar cell on a rigid soda-lime glass (SLG) substrate is 12.6% [4], the efficiencies of flexible CZTSSe solar cells are relatively low (below 10%). Recently, Yang et al. [18] reported the highest PCE of 10.34% for a flexible CZTSSe solar cell; this cell was fabricated on a Mo foil substrate with a sodium fluoride (NaF) doping layer.

Sodium (Na) doping of CZTS and $\text{Cu}_2\text{ZnSnSe}_4$ (CZTSe) thin-film solar cells resulted in increased grain size, open-circuit voltage (V_{OC}), and fill factor (FF) [19,20]. Moreover, the cell performances of the CZTS and CZTSe thin-film solar cells can be improved through Na doping. Prabhakar et al. [21] and Li et al. [22] found that Na diffusion increased the hole carrier concentrations in the CZTS and CZTSe thin-film solar cells, respectively, which increased the conductivity and in turn influenced V_{OC} and PCE. Although little research has been conducted on the effect of Na doping on the CZTSSe thin-film solar cells, Fella et al. [23] demonstrated that the incorporation of an NaF top layer with an optimal thickness into the CZTSSe thin-film solar cell increases both V_{OC} and FF. They also demonstrated that adjusting the sodium precursor quantity enables tuning of doping levels and gradients to maximize the collection of photogenerated carriers. Moreover, the incorporation of the NaF layer in the kesterite solar cells results in enhanced V_{OC} and carrier separation at grain boundaries (GBs) [24,25]. In particular, Na incorporation hindered the formation of secondary phases and passivated defects [26–28]. Maeda et al. [29] demonstrated that some Na atoms can substitute the Cu and Zn atoms to form Na_{Cu} and Na_{Zn} , respectively, when the CZTS and CZTSe films are annealed at high temperatures in S or Se atmosphere with post-deposition of a sodium compound. The formation energies Na_{Cu} and Na_{Zn} are quite low; therefore, they can be formed relatively easily compared to detrimental Sn_{Zn} defects. Lin et al. [30] reported that bifacial Na incorporation passivated deep defect states near the CZTS/CdS junction, improved the carrier collection efficiency, and lowered the recombination loss. Various Na doping methods have been used to improve the performance of flexible kesterite thin-film solar cells, as summarized in Table 1.

The photo-induced properties of Na-incorporated CZTSSe thin-film solar cells have not been thoroughly investigated. To better understand the effect of Na doping on the properties of flexible CZTSSe thin-film solar cells, we characterized the optoelectronic properties of CZTSSe absorber layers by investigating their surface potential distributions near the GBs. The CZTSSe thin films were deposited on the Mo foil substrates with NaF doping layers with varying thicknesses to determine the optimal amount of Na required to maximize the performance of the CZTSSe absorber layer. The amount of Na remaining on the absorber surface strongly affected the PCEs of the solar cells, which range from 0.69% to 8.66%. Our cell, with the highest PCE, displayed promising performance compared to that of other solar cells with flexible substrates and sodium doping. The cell with the highest PCE had a slightly higher FF (62.63%) than that of a previously reported CZTSSe thin-film solar cell (PCE = 10.34%, FF = 57.2%) [18]. The highest PCE of our cell was ~2% higher than that of a flexible glass CZTSSe thin-film solar cell with the same thickness of the NaF layer deposited using the electron-beam evaporation method (PCE = 6.3%) [13]. Moreover, the best efficiency of our cell achieved higher PCE through Na doping compared to other Mo foil substrate CZTSSe solar cells. Compared to other flexible CZTSSe solar cells fabricated on Mo foil using metallic precursors including MgF_2 anti-reflective coating, the best performance of our cell showed ~1% higher PCE through Na doping [17,31]. Specific cell structure is shown in Table 1.

Table 1
Comparison of kesterite thin-film solar cells.

Substrate	Absorber material	Solar cell structure (*AR coating)	Na doping method	PCE ^a (%)	Ref.
SLG	CZTSSe	SLG/Mo/CZTSSe/CdS/ZnO/ITO:Al/ MgF_2	Undoped	12.6	[4]
Mo foil	CZTSSe	Mo foil/CZTSSe/CdS/i-ZnO/AZO/Al	NaF, thermal evaporation	10.34	[18]
	CZTSSe	Mo foil/CZTSSe/CdS/i-ZnO/ITO/Ag	Annealing with soda-lime glass	6.78	[16]
	CZTSSe	Mo foil/CZTSSe/CdS/i-ZnO/AZO/Al/ MgF_2	Undoped	8	[17]
	CZTSSe	Mo/CZTSSe/CdS/i-ZnO/AZO/Ni/Al/ MgF_2	Undoped	7.1	[31]
Al foil	CZTSSe	Mo foil/CZTSSe/CdS/i-ZnO/AZO/Ni/Al/ MgF_2	NaF, e-beam evaporation	8.66	This work
	CZTS	Al foil/Mo/CZTS/ZnS/i-ZnO/ITO/Ni/Al	Undoped	1.94	[32]
Ti foil	CZTSSe	Ti foil/CZTSSe/CdS/i-ZnO/ITO	Undoped	2.00	[14]
Stainless steel	CZTS	SS430/Mo/CZTS/CdS/ZnO/ITO	MoNa, sputtering	6.29	[33]
	CZTS	SS430/Ti/Mo/CZTS/CdS/i-ZnO/ITO	NaF, sputtering	4.10	[34]
	CZTSe	SS430/Cr/Mo/Mo:Na/Mo/i-ZnO/CZTSe/CdS/ZnO/ Sn_2O_3 :In	MoNa, sputtering	4.30	[35]
Polyimide	CZTSe	SS/Cr/Mo/ZnO/CZTSe/CdS/i-ZnO/ZnO:Al	Undoped	3.50	[36]
	CZTS	PI/Mo/CZTS/CdS/ZnO:Al/Al-grid	Undoped	0.49	[37]
Flexible glass	CZTSSe	Willow Glass/Mo/CZTSSe/CdS/ZnO/ITO/Al–Ni grid	Undoped	6.90	[13]

^a PCE: power conversion efficiency.

2. Experimental methods

2.1. Fabrication of CZTSSe thin-film solar cell

Fig. 1(a) and (b) show the fabrication process of a CZTSSe solar cell on the Mo foil and photograph of the resultant device, respectively. The metal precursor layers of the CZTSSe absorber layer were grown on 0.1 mm-thick flexible Mo foil with a stacking order of Sn/Cu/Zn/Mo [38]. The Zn and Cu layers were deposited via direct-current (DC) magnetron sputtering, and the Sn layer was deposited by radio-frequency (RF) magnetron sputtering. In all the cases, the sputtering power was 50 W (1.1 W/cm^2) in an argon atmosphere. Next, an NaF layer with a thickness of 5, 10, 25, or 30 nm was deposited on the precursor layers by electron-beam evaporation. The sulfo-selenization process of the precursor layers was conducted by rapid thermal annealing (RTA) using SeS_2 and Se powders with an SeS_2/Se ratio of 0.08% in an Ar-filled graphite box at atmospheric pressure. Before the thermal annealing treatment, the RTA chamber was evacuated for 3 min using a rotary

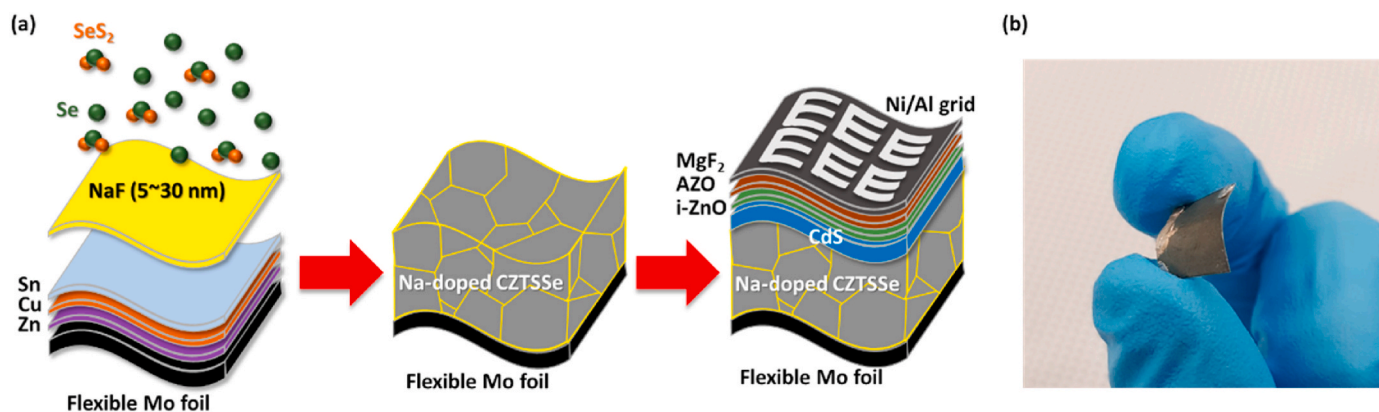


Fig. 1. (a) Diagram of the fabrication process of a thin-film solar cell with a kesterite ($\text{Cu}_2\text{ZnSn}(\text{S},\text{Se})_4$; CZTSSe) polycrystalline absorber layer. After Zn, Cu, and Sn metallic precursor layers were deposited on flexible Mo foil by sputtering, an NaF layer was deposited for Na doping. The layered sample was annealed in an atmosphere of Se and SeS_2 to form an Na-doped CZTSSe absorber layer. After that, intrinsic ZnO, aluminium-doped ZnO and MgF_2 anti-reflecting layers were deposited. (b) Photograph of a flexible CZTSSe thin-film solar cell.

pump, and the chamber was filled with argon gas to atmospheric pressure. Thereafter, maintaining the atmospheric pressure, the precursors were heated from room temperature to $300\text{ }^\circ\text{C}$ in 1000 s, and this temperature condition was maintained for 1500 s. From $300\text{ }^\circ\text{C}$, the precursors were heated to $560\text{ }^\circ\text{C}$ in 1000 s and then maintained at $560\text{ }^\circ\text{C}$ for 1100 s.

After RTA, the resulting CZTSSe absorbing layer was immersed in an aqueous KCN solution to remove any secondary phase(s) present. It is well known that KCN etching plays a role in removing the secondary phase, particularly Cu-related binary phase [39]. Recently, Benhaddou et al. reported that KCN etching also leads to improvement of p-n junction through the reduction of non-radiative recombination in $\text{Cu}_2\text{ZnGeSe}_4$ -based solar cells [40]. In the chalcogenide case, Colombara et al. recently demonstrated that KCN etching selectively removes the Cu–Se secondary phase in CuInSe (CIS); however, additional recombination or trapping pathway was induced, which can be passivated by oxygen incorporation [41]. A 70 nm-thick CdS buffer layer was fabricated by chemical bath deposition, and a 50 nm-thick intrinsic ZnO layer and a 300 nm-thick Al-doped ZnO window layer were deposited by RF magnetron sputtering. Next, 50 nm-thick Ni and 500 nm-thick Al electrodes were deposited by electron-beam evaporation using a shadow mask. A 130 nm-thick MgF_2 anti-reflective coating was deposited on the samples. Solar cell parameters of samples are reported in Table 2. Though the CZTSSe absorbers contained different amount of Na before the annealing process, the annealing conditions were applied identically for all the samples. The different amount of sodium affected in stoichiometry, the final compositional ratios of the CZTSSe absorber layers are shown in Table S1 in Supporting Information.

2.2. Characterization of illumination-induced properties of solar cells

The electrical characteristics of the absorber surface were characterized by Kelvin probe force microscopy (KPFM). Surface photovoltage (SPV) measurements were conducted by laser-assisted KPFM. Using

Table 2

Solar cell parameters of samples in planar state obtained from the J–V curves and EQE data. Active area is 0.187 cm^2 .

Sample	PCE (%)	$J_{SC, J-V}$ (mA/cm^2)	V_{OC} (V)	FF (%)	$J_{SC, EQE}$ (mA/cm^2)	E_g (eV)	$E_g/q-V_{OC}$ (V)
Na_1	0.69	13.97	0.176	27.88	15.93	1.18	1.004
Na_2	4.56	29.96	0.337	45.15	29.75	1.16	0.823
Na_3	8.66	32.27	0.428	62.63	32.04	1.15	0.722
Na_4	7.19	30.99	0.427	54.27	31.15	1.16	0.733

KPFM, the surface potential of the CZTSSe absorber layer was measured in a non-contact mode with a 40 nm set point using a platinum (Pt)/iridium (Ir)-coated silicon (Si) tip. The scan region was $4 \times 4\text{ }\mu\text{m}$ and the scan rate was under 0.2 Hz. A commercial atomic force microscope (AFM; n-Tracer, NanoFocus Inc.) was used for the KPFM measurements. The SPV measurements were conducted by exciting the sample with lasers with wavelengths of 405, 532, and 640 nm, which had energies of 1.94, 2.33, and 3.06 eV, respectively, at a power of 10 mW. According to the ratio of the amount of Na remaining on the surface of the absorber layer, the samples were denoted as Na_1 (0.95%), Na_2 (3.85%), Na_3 (5.05%), and Na_4 (7.35%). The absolute quantity of Na remaining on the surface was measured by X-ray photoelectron spectroscopy; the data are provided in Supporting Information (Fig. S1 and Table S2).

3. Results and discussion

3.1. Kelvin probe force microscopy measurements under dark conditions

To investigate the effect of the Na content on the surface of the CZTSSe absorber layer on its electrical properties, surface potential maps and surface topographies were obtained via KPFM. Fig. 2(a1–d1) and (a2–d2) show the surface topography and surface potential maps, and all the NaF-doped samples showed higher potential in the GB regions than in the intra-grain (IG) regions, which is equivalent to the downward band bending at the GBs. The formation of a higher surface potential at the GBs than at IG regions demonstrates the existence of a local built-in potential at the GBs acting as a hole barrier [42]. Therefore, majority carriers are repelled to the IG regions and minority carriers are attracted to the GBs by the presence of an electric field in the vicinity of the GBs. Li et al. [43] demonstrated the formation of a higher surface potential at the GBs than at the IG regions in the CZTSSe thin-film solar cells. Moreover, previous studies have illustrated that a large upward potential bending at the GBs facilitates carrier separation and minority carrier transport [44,45]. Here, holes, which are the majority carrier in p-type CZTSSe absorber layers, are repelled to the IG regions and electrons accumulate at the GBs.

Surface potential values were extracted from 25 randomly chosen GBs and IG regions on each surface potential map. Fig. 2(a3–d3) and (a4–d4) show the histograms of the surface potentials at 25 GBs and IG regions, respectively, for samples Na_1 to Na_4. A positively charged surface potential was formed at the GBs, and a negatively charged surface potential was formed in the IG regions, except for at a few locations. The average potential at the GBs and IG regions depended on the Na content of the sample. As the amount of Na remaining on the surface increased, the average potential increased. Sample Na_4 showed the

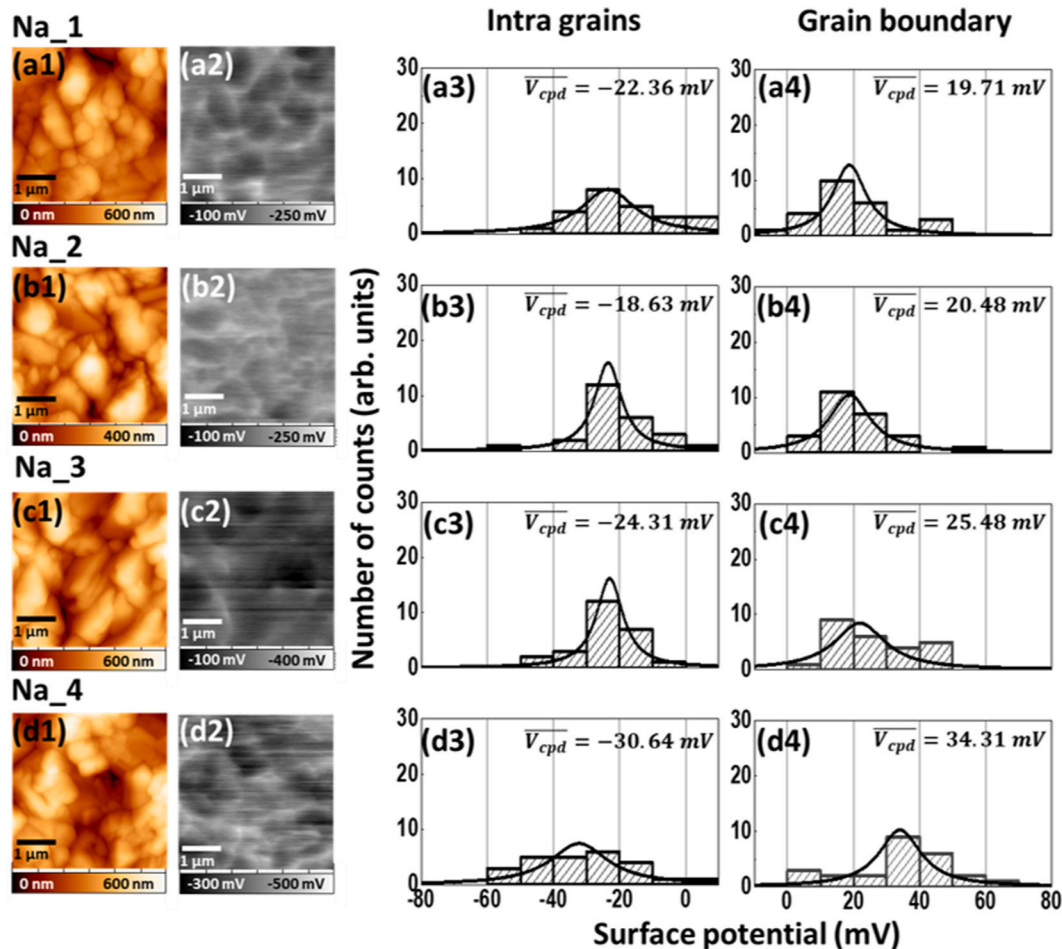


Fig. 2. (a1–d1) Surface topography and (a2–d2) surface potential maps of planar state absorber layers (a) Na₁, (b) Na₂, (c) Na₃, and (d) Na₄ obtained by Kelvin probe force microscopy under dark conditions. Histograms of surface potential at 25 randomly selected (a3–d3) intra-grain regions and (a4–d4) grain boundaries under dark conditions. The black curves represent surface potential distributions.

highest and lowest potentials of 34.41 and -30.64 mV among all the samples at the GBs and IG regions, respectively. The difference between the average surface potentials at the GBs and IG regions increased with the amount of Na of the absorber layer. Therefore, a deeper downward band bending at the GBs occurred as the Na surface coverage increased. Deep band bending attracts more electrons and acts as a stronger hole barrier compared with the case for shallow band bending [43]. Moreover, Na segregation increases the potential difference between the GBs and IG regions, which increases the electrostatic force at the GBs. Jiang et al. [46] and Yan et al. [47] suggested that on the chalcogenide thin-film surfaces, the presence of Na at the GBs induces a larger increase in the surface potential than that in the Na-free areas. A higher Na content also increases the hole concentration by lower the thermal activation energy, which leads to a higher built-in voltage [48]. Thus, the high potential difference between the GBs and IG regions increases the electrostatic force at the GBs and subsequently leads to a higher built-in voltage. Moreover, a previous study revealed that the optimized doping leads to sufficient built-in potential and selection of a better carrier transport path by comparing the built-in potential calculated from the capacitance–voltage measurement and the conduction path [38].

3.2. Photo-assisted Kelvin probe force microscopy measurements

Fig. 3(a1–d1) show the surface topography and Fig. 3(a2–d2)–(a4–d4) show the surface potential maps under various illuminated conditions (405, 532, and 640 nm). In Fig. 3(a5–d5)–(a6–d6), the

surface potentials were extracted from 25 randomly selected GBs and IG regions from samples Na₁ to Na₄ under 640 nm illumination to investigate the illumination-induced changes in the surface potential of the Na-doped CZTSSe absorber layers. For each sample, the average potential at the GBs and IG regions under illumination differed compared to that under dark conditions. The samples with sufficient Na content (Na₃ and Na₄) showed a higher average potential at the GBs and a lower average potential at the IG regions, as was observed under dark conditions.

The average surface potential increased or decreased under illumination compared to that in the dark because of carrier excitation. The average surface potential at the GBs of sample Na₂ decreased from 20.48 mV in the dark to 19.89 mV under 640 nm illumination. In samples Na₃ and Na₄, the average surface potential at the GBs increased by 12.47 and 0.34 mV, respectively, compared with that in the dark, which means that a deeper downward band bending occurred at the GBs under illumination compared with the case in the dark. A previous study observed enhancement of photogenerated carrier transport under illuminated condition with varying Na content [49]. An increased surface potential was also observed under illumination at 532 and 405 nm (Fig. S3). The difference between the average surface potentials at the GBs and IG regions was most pronounced in sample Na₄, which showed a value of 67.78 mV. Considering that the average surface potential difference between the GBs and IG regions was 49.79 mV in Na₃ in the dark, samples Na₃ and Na₄ showed increased band bending at the GBs under illumination compared with that in the dark. Thus, Na doping enhanced the carrier separation at the GBs, which should in turn

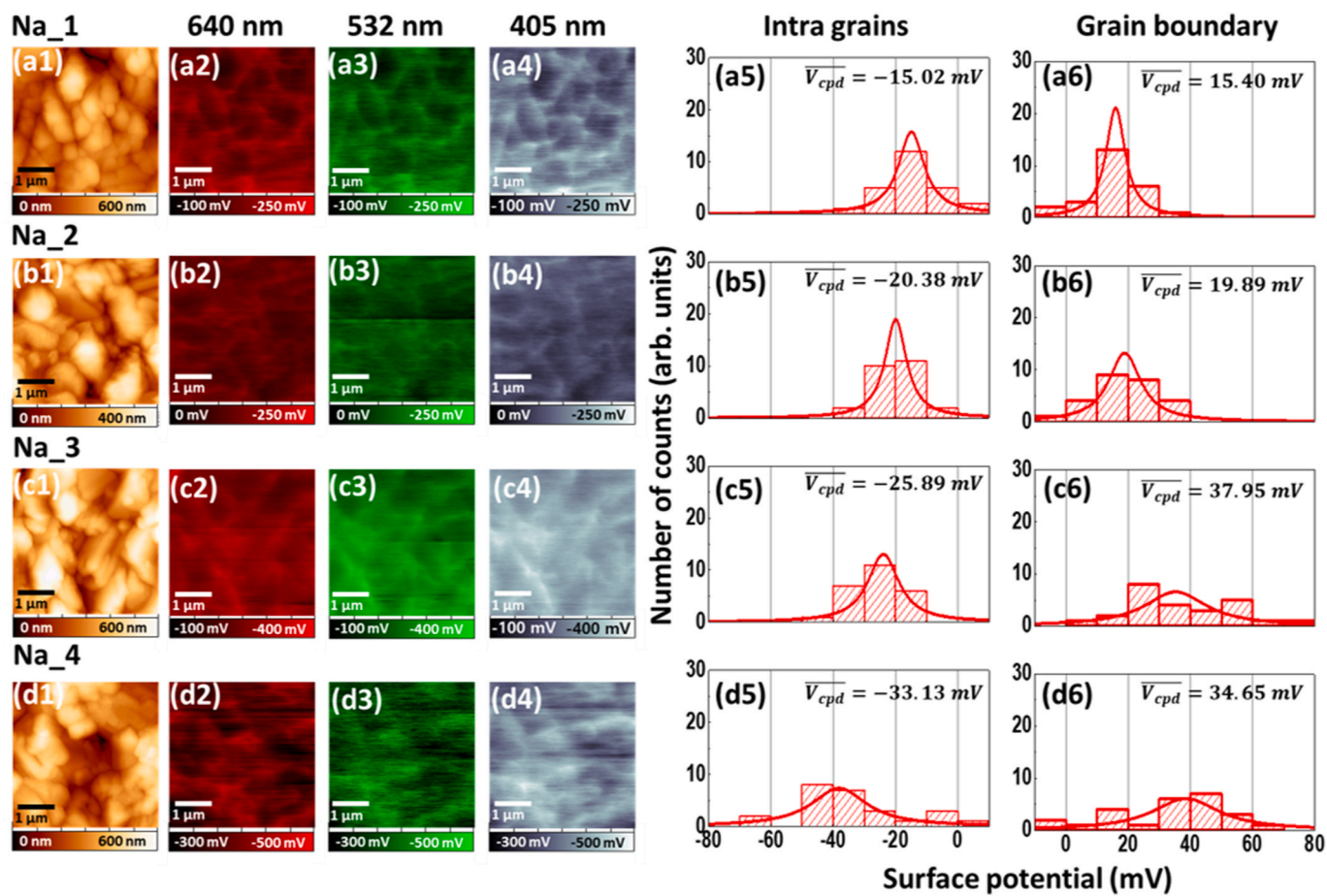


Fig. 3. (a1–d1) Surface topography and surface potential maps of planar state absorber layers (a) Na₁, (b) Na₂, (c) Na₃, and (d) Na₄ under illumination at (a2–d2) 640 nm, (a3–d3) 532 nm, and (a4–d4) 405 nm. Histograms of surface potential from 25 randomly selected (a5–d5) intra-grain regions and (a6–d6) grain boundaries under 640-nm illumination. The red curves represent surface potential distributions.

improve the cell performance [46].

The SPV measurements were obtained by photo-assisted KPFM. Fig. 4(a)–(d) show the work function distributions of the CZTSSe absorber films determined from the corresponding surface potential maps. The number of counts was normalized for all the distributions.

The work functions of the CZTSSe absorber layers with different Na contents were obtained under both dark and illuminated conditions to investigate their band structures. The work function of each sample was calculated using contact potential difference (V_{cpd}) as follows:

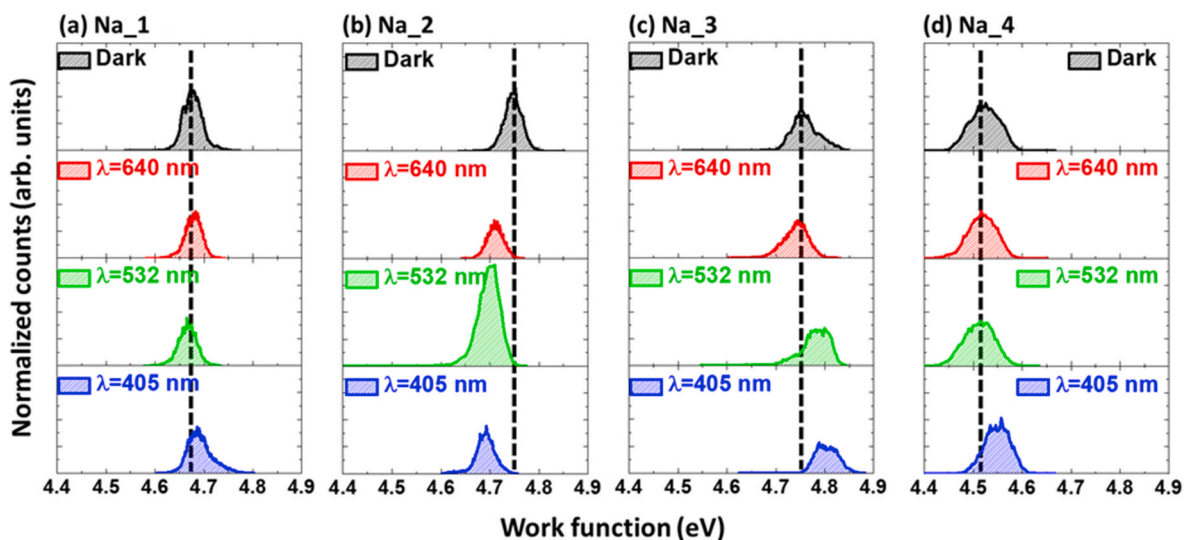


Fig. 4. Work function distributions of planar state CZTSSe absorber layers (a) Na₁, (b) Na₂, (c) Na₃, and (d) Na₄ calculated from surface potentials under illumination at different wavelengths. The black dotted line indicates the location of peak work function in the dark state.

$$V_{cpd, sample} = \frac{\phi_{tip} - \phi_{sample}}{-e} \quad (1)$$

where ϕ_{tip} and ϕ_{sample} are the work functions of the Pt/Ir-coated tip and sample, respectively. The change in the work function for each sample under different illuminated conditions is shown in Fig. S4. A wide work function distribution with more than one peak indicates the presence of a secondary phase such as ZnSe [50]. None of our samples displayed a wide peak, indicating that no secondary phase was present.

As shown in Fig. 4(a), the work function distribution of sample Na₁ was not strongly affected by all the illumination conditions (under 405, 532, and 640 nm wavelength), implying that SPV formation was limited. Here, SPV generation was limited by carrier recombination, which led to minority carrier loss. In the CZTSSe thin-film solar cells, the defects in bulk CZTSSe acted as recombination centers by forming a mid-gap state and non-uniform chemical stoichiometry or structure, which caused V_{OC} to decrease [26,51,52]. Na is known to passivate defects [19,30,53]. The segregation of defects such as Zn_{Sn} , O_{Se} , and Na_i at the GBs is beneficial because: (i) bond weakening or breakage results in deep levels in CZTSSe, and (ii) it facilitates electron transport through the GBs by creating hole barriers and electron sinkers, thereby promoting effective charge separation at the GBs. In addition, Na doping suppresses the recombination of the minority carriers by passivating the donor defects such as Zn_{Cu} and Sn_{Cu} [54]. Na doping has been reported to suppress GB-originated defects and shift deep defects caused by S antibonding closer to the Fermi level [55]. Sun et al. [56] demonstrated that an Na-doped film surface should be Zn-rich and have a lower density of detrimental $[2Cu_{Zn} + Sn_{Zn}]$ defect clusters compared with the case for an undoped CZTSSe absorber layer. Han et al. [57] reported that Na doping suppressed Sn_{Zn} , which is a deep recombination center and mid-gap state, because Na_{Zn} is preferentially formed rather than Sn_{Zn} owing to lower formation energy of Na_{Zn} . Na doping also suppresses the formation of Zn_{Sn} defects, which can be detrimental recombination sites. Therefore, the formation of deep recombination centers is suppressed by the Na-based defects such as Na_{Zn} . In the samples with low Na content, the Na passivation effect is negligible; therefore, the photogenerated carriers are trapped at the defect sites and the SPV is low. Except for sample Na₂, there was no significant work function shift under 640 nm wavelength illuminated condition. The SPV of sample Na₂ showed a negative shift under illumination compared with that in the dark. The negative shift of V_{cpd} implies a decrease in the Fermi level and increase in hole density [58].

The work function distributions of samples Na₃ and Na₄ showed positive shifts under illumination compared with those in the dark. Such work function shifts indicate that the presence of sufficient Na in samples Na₃ and Na₄ enables effective defect passivation, which leads to suppressed recombination and higher SPV. Under 405 nm laser illumination, the work function distribution shifted by approximately 46 and 26 meV in samples Na₃ and Na₄, respectively, which are the largest shifts among the three illumination wavelengths investigated. The illuminated wavelength affected the photo-induced defect passivation, resulting in different magnitudes of the SPV. For example, the defects that act as carrier traps can be occupied by electrons generated by blue photons, compensating the defect state [59–61]. Thus, the negative effect of the recombination sites was suppressed by blue illumination, which contributed to the formation of a large SPV. The SPV is calculated as

$$SPV = V_{cpd, illuminated} - V_{cpd, dark} \quad (2)$$

Several studies have revealed that positive SPV generation indicates *p*-type materials' nature [62,63].

Previous studies demonstrated that the Na ions diffuse and are active along the GBs rather than the IG regions in a kesterite thin film [27,64,65]. Moreover, a lower work function of a high Na content sample can be attributed to the surface dipoles induced by Na, which resulted in a large built-in potential [44,66]. In our CZTSSe thin-film solar cells, no

Na-related clusters due to excessive Na were detected. Therefore, excessive Na ions in sample Na₄ may be distributed over the absorber surface in addition to the accumulation at the GBs and a lower work function. The Na ions were distributed vicinity of GBs passivating the defects in the optimal Na sample, whereas excessive Na ions in sample Na₄ were more distributed over the surface, resulting in lower defect passivation at the GBs than in the optimal Na sample.

3.3. Carrier transport in Na-doped CZTSSe absorber layers

Fig. 5(a) shows a diagram of a kesterite unit cell, and Fig. 5(b), (c) show the energy-band diagram of the surface of an CZTSSe absorber layer with and without Na passivation, contacting with a metal tip in the dark and under illumination conditions. The carrier excitation of the sample with Na passivation strongly depended on the incident energy, as confirmed by the surface potential distribution shift (Fig. 4). In contrast, carrier excitation was not strongly affected by the incident energy in the case of the Na-deficient sample Na₁. As shown in Fig. 5(b), in the samples with low Na content, the photogenerated carriers are trapped at the defect sites and the formation of SPV is limited. In contrast, in the Na-sufficient samples, defects are passivated and recombination is suppressed; therefore, the photogenerated carriers exhibit large SPVs, as shown in Fig. 5(c).

Leibovitch et al. [68] reported that photogenerated band bending affected the contact potential difference regardless of its depth in a sample. The direction of band bending at a surface can be determined by tuning the work functions of the metal tip and semiconductor materials [69]. Moreover, the movement direction of the excited carriers depends on the surface band bending [58]. The work function of the Pt/Ir-coated Si tip used here is 4.9 eV, which is higher than that of the CZTSSe absorber layer. Therefore, the bands at the GBs of the Na-deficient CZTSSe absorber layer are bent upward, forming a Schottky barrier with the Pt/Ir-coated Si tip. The degree of upward band bending decreases under illumination compared with that in the dark. Conversely, band bending at the GBs occurred in the opposite direction in the Na-sufficient samples (Na₃ and Na₄). As discussed above, the CZTSSe absorber layer shows downward band bending at the GBs because of the higher work function at the GBs than in the IG regions. Assuming that the Fermi level is in equilibrium at the interface between the GBs and IG regions, because the valence band level of the GBs shows downward bending, the distance between the Fermi level and valence level increases. Therefore, the bands at the GBs of the Na-sufficient CZTSSe absorber layers bend downward. According to the SPV theory, in this regime of surface band bending, illumination causes surface band bending to weaken [70,71]. Therefore, because of the electric field, the photogenerated electrons move toward the surface and holes shift away from the surface and toward the bulk region in materials with downward band bending. The negative charge accumulation resulting from electron concentration on the surface neutralizes and screens the positively charged donor-type surface states [71]. The surface defects were passivated by the presence of sufficient Na in samples Na₃ and Na₄, which indicates that the amount of charge accumulated by the excited electrons was greater than that in the case of the Na-deficient samples. This charge accumulation induced an increase in the Fermi level in the samples with sufficient Na doping, which resulted in a well-aligned junction with a buffer layer.

Herein, all the characterizations of the CZTSSe absorber layers were performed when the samples were in the planar state. However, to maximize the practical use of flexible CZTSSe solar cells, understanding the change due to the bending is required. Therefore, bending test has been done to check the bending stability of the flexible CZTSSe thin film solar cells. After 1000 bending cycles with 12 mm bending radius, the randomly chosen nine flexible CZTSSe thin film solar cell samples maintained 92.2% of their performance. Bending test results are shown in Fig. S7 in Supporting Information. If the crystal structure of the cell is broken through mechanical bending, the grain and GB properties will

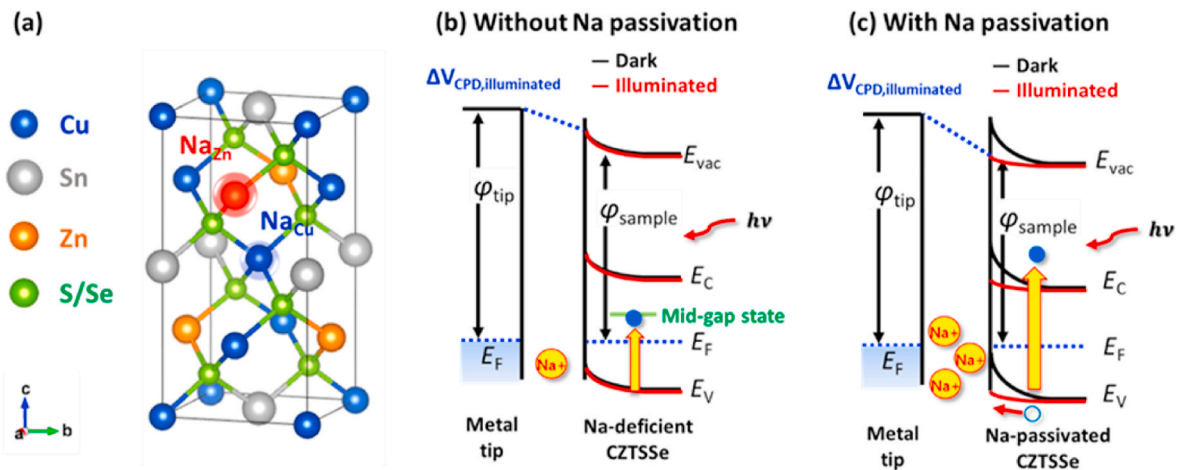


Fig. 5. (a) Diagram of a kesterite unit cell with a Na_{Zn} and Na_{Cu} by Na incorporation and (b–c) energy-band diagram of the interface between a CZTSSe absorber layer and metal tip with and without Na passivation. E_{vac} and E_F are the vacuum level and Fermi level, respectively. E_C and E_V are the conduction band edge and valence band edge, respectively. ϕ indicates work function. Blue solid circles and open circles are electrons and holes generated by additional energy, respectively. Yellow solid circles indicate Na ions accumulated at GBs. The blue dotted line is the quasi-Fermi level. VESTA software was used for diagram [67].

change and result in the change of conduction path of the minority carriers, which can lead to the selection of a worse conduction path. Therefore, band bending at the GBs will decrease. As the carrier collection at the GBs decreases, a decreased built-in potential will result in a decrease in the efficiency. Moreover, although the migration of Na ions with mechanical bending is not clearly revealed yet, if the Na ions move from the GBs to IG regions, then the passivation effect on the defects at the GBs will decrease and result in a small SPV. The behavior of the charge in the bending state is an issue that needs to be considered.

The Na content strongly affected the solar cell parameters and stoichiometry, as shown in Table 2 and Table S1. Box plots and the solar cell parameters of the nine solar cells are shown in Fig. S5 and Table S3 in Supporting Information. To maximize the PCE and short-circuit current (J_{SC}), MgF₂ anti-reflective coating was applied here [72]. Compared to the flexible CZTSSe thin film solar cells containing Na without usage of anti-reflective coating [16], J_{SC} was improved substantially with usage of MgF₂ anti-reflective coating. Herein, the improved efficiency of our cell was achieved through incorporation of Na compared to the Mo substrate flexible CZTSSe thin film solar cells including MgF₂ anti-reflective coating without the incorporation of Na [17,31]. J_{SC} , FF, and PCE of the devices increased with the increasing Na content and decreased in sample Na₄ with V_{OC} value saturation though the sample Na₄ showed the highest Zn/Cn and the lowest Cu/(Zn + Sn) compositional ratio. As shown in Table S1, Na doped CZTSSe absorber samples showed Zn-rich and Cu-poor stoichiometry which is beneficial for kesterite device properties since Cu-poor stoichiometry showed less Cu/Zn disorder than Cu-rich stoichiometry [57,73].

The E_g values were obtained from external quantum efficiency (EQE), and the V_{OC} deficits were calculated based on the relationship between E_g and V_{OC} , $\frac{E_g}{q} - V_{OC} \propto A \ln n$, where A is the diode ideality factor and n is the concentration of the recombination centers. The V_{OC} deficit decreased with the increasing Na content and increases marginally in sample Na₄ along with the PCE. The difference in J_{SC} and V_{OC} between samples Na₃ and Na₄ was marginal; therefore, improvement of the V_{OC} deficit is crucial to attain a high efficiency. Moreover, though the difference in the J_{SC} values between samples Na₂ and Na₄ was only 1.03 mA/cm², the V_{OC} and PCE decrease significantly; therefore, defect-related V_{OC} losses affected the PCE drop critically. Significant V_{OC} shortfall can be attributed mainly to the recombination by deep-level defects; therefore, the V_{OC} deficit can be decreased by controlling the of defect formation and defect passivation [74,75]. In addition, the cell with the highest efficiency had a slightly higher FF than that of the recorded cell that had a similar bandgap with a 10 nm thickness of NaF

(FF = 57.2%, E_g = 1.12 eV) [18]. A higher FF achieved through the selection of a better carrier transport path, and an enhanced built-in potential due to optimal Na doping affects the FF [38].

In Table 2, sample Na₁ shows the largest V_{OC} deficit and has the least magnitude of SPV formation. Moreover, this Na-deficient sample shows the highest V_{OC} deficit due to the high concentration of the recombination centers with low defect passivation. Except for under the illuminated condition of 405 nm wavelength, sample Na₄ did not have a higher SPV compared to sample Na₃, which implies the saturation of the defect passivation effect. Sample Na₄ showed the higher V_{OC} deficit even though it has more Zn-rich and Cu-poor stoichiometry than the sample Na₃. SPV saturation was coherent with V_{OC} saturation because the defect passivation mainly affects the improvement of V_{OC} [19]. Moreover, defect passivation in sample Na₄ was saturated since the Na ions were distributed over the surface in addition to the GBs. In addition, excessive Na can result in a poor p-n junction with the CdS buffer layer, leading to deteriorated efficiency [23]. In conclusion, maximized defect passivation by optimal Na content leads to the maximum efficiency of the cell.

4. Conclusions

The effect of Na doping on GBs and photo-induced properties of CZTSSe thin-film solar cells were studied via photo-assisted KPFM. CZTSSe absorber layers with different Na doping amounts were deposited on a flexible Mo foil using a metal precursor. The Na doping enhanced the photogenerated carriers and increased the electrostatic force at the GBs. The samples with sufficient Na doping content showed a positive shift in the work function with a maximum value of 46 meV under 405-nm illumination owing to suppressed recombination by defect passivation. The work function shift was smaller for samples with lower Na doping content because of the low passivation effect. Defect passivation induced by blue photon (405 nm wavelength) was also observed; this effect was the largest in the sample with the optimal Na content. Thus, the photo-induced characteristics of the CZTSSe absorber layers were strongly influenced by the Na doping. We believe that Na doping promotes defect passivation on the CZTSSe absorber surface and will finally lead to the formation of an improved p-n junction with buffer layer, hindering V_{OC} losses. Examining the photo-induced properties of the CZTSSe absorber layers will help us maximize their practical performance.

CRediT authorship contribution statement

Ha Kyung Park: Conceptualization, Visualization, Data curation, Formal analysis, Investigation, Writing – original draft. **Yunae Cho:** Formal analysis, Investigation, Writing – review & editing. **Juran Kim:** Formal analysis, Investigation. **Gee Yeong Kim:** Formal analysis, Investigation. **Woo-Lim Jeong:** Resources, Investigation. **Kyung-Pil Kim:** Resources, Investigation. **Dong-Seon Lee:** Supervision, Validation, Writing – review & editing. **William Jo:** Supervision, Validation, Project administration, Writing – review & editing.

Declaration of competing interest

The authors declare that they have no known competing financial interests or personal relationships that could have appeared to influence the work reported in this paper.

Acknowledgments

This research was supported by Basic Science Research Program through the National Research Foundation of Korea (NRF) funded by the Ministry of Education (NRF-2018R1A6A1A03025340, 2018R1A2B2003607, and 2020R111A1A01068700); and this work was supported by grant (2016M1A2A2936784) of the Technology Development Program for the solving of climate change, which was provided through the National Research Foundation (NRF). Moreover, it was supported by the GIST Research Institute (GRI) in 2021. The first author Ha Kyung Park is also grateful for the financial support received from the Hyundai Motor Chung Mong-Koo foundation.

Appendix A. Supplementary data

Supplementary data to this article can be found online at <https://doi.org/10.1016/j.solmat.2021.111243>.

References

- S. Siebentritt, S. Schorr, Kesterites—a challenging material for solar cells, *Prog. Photovolt.* 20 (2012) 512–519, <https://doi.org/10.1002/ppp.2156>.
- J.J. Scragg, P.J. Dale, L.M. Peter, Towards sustainable materials for solar energy conversion: preparation and photoelectrochemical characterization of $\text{Cu}_2\text{ZnSnS}_4$, *Electrochem. Commun.* 10 (2008) 639–642, <https://doi.org/10.1016/j.elecom.2008.02.008>.
- F. Luckert, D.I. Hamilton, M.V. Yakushev, N.S. Beattie, G. Zoppi, M. Moynihan, I. Forbes, A.V. Karotki, A.V. Mudryi, M. Grossberg, J. Krustok, R.W. Martin, Optical properties of high quality $\text{Cu}_2\text{ZnSnSe}_4$ thin films, *Appl. Phys. Lett.* 99 (2011), 062104, <https://doi.org/10.1063/1.3624827>.
- W. Wang, M.T. Winkler, O. Gunawan, T. Gokmen, T.K. Todorov, Y. Zhu, D.B. Mitzi, Device characteristics of CZTSSe thin-film solar cells with 12.6% efficiency, *Adv. Energy Mater.* 4 (2014) 1301465, <https://doi.org/10.1002/aenm.201301465>.
- M. Nakamura, K. Yamaguchi, Y. Kimoto, Y. Yasaki, T. Kato, H. Sugimoto, Cd-free $\text{Cu}(\text{In,Ga})(\text{Se,S})_2$ thin-film solar cell with record efficiency of 23.35%, *IEEE J. Photovolt.* 9 (2019) 1863–1867, <https://doi.org/10.1109/JPHOTOV.2019.2937218>.
- T. Kato, J.-L. Wu, Y. Hirai, H. Sugimoto, V. Bermudez, Record efficiency for thin-film polycrystalline solar cells up to 22.9% achieved by Cs-treated $\text{Cu}(\text{In,Ga})(\text{Se,S})_2$, *IEEE J. Photovolt.* 9 (2019) 325–330, <https://doi.org/10.1109/JPHOTOV.2018.2882206>.
- S. Siebentritt, Why are kesterite solar cells not 20% efficient? *Thin Solid Films* 535 (2013) 1–4, <https://doi.org/10.1016/j.tsf.2012.12.089>.
- T.K. Todorov, J. Tang, S. Bag, O. Gunawan, T. Gokmen, Y. Zhu, D.B. Mitzi, Beyond 11% efficiency: characteristics of state-of-the-art $\text{Cu}_2\text{ZnSn}(\text{S,Se})_4$ solar cells, *Adv. Energy Mater.* 3 (2013) 34–38, <https://doi.org/10.1002/aenm.201200348>.
- A. Chirila, P. Reinhard, F. Pianezzi, P. Bloesch, A.R. Uhl, C. Fella, L. Kranz, D. Keller, C. Gretener, H. Hagendorfer, D. Jaeger, R. Erni, S. Nishiwaki, S. Buecheler, A.N. Tiwari, Potassium-induced surface modification of $\text{Cu}(\text{In,Ga})\text{Se}_2$ thin films for high-efficiency solar cells, *Nat. Mater.* 12 (2013) 1107–1111, <https://doi.org/10.1038/nmat3789>.
- A. Kampmann, J. Rechid, A. Raitzig, S. Wulff, M. Mihailova, R. Thyen, K. Kalberlah, Electrodeposition of CIGS on metal substrates, *Mater. Res. Soc. Symp. Proc.* 763 (2003) 323–328, <https://doi.org/10.1557/PROC-763-B8.5>.
- M. Patel, A. Ray, Enhancement of output performance of $\text{Cu}_2\text{ZnSnS}_4$ thin film solar cells—a numerical simulation approach and comparison to experiments, *Physica B* 407 (2012) 4391–4397, <https://doi.org/10.1016/j.physb.2012.07.042>.
- K. Herz, A. Eicke, F. Kessler, R. Wächter, M. Powalla, Diffusion barriers for CIGS solar cells on metallic substrates, *Thin Solid Films* 431 (2003) 392–397, [https://doi.org/10.1016/S0040-6090\(03\)00259-1](https://doi.org/10.1016/S0040-6090(03)00259-1).
- K.W. Brew, S.M. McLeod, S.M. Garner, R. Agrawal, Improving efficiencies of $\text{Cu}_2\text{ZnSnS}_4$ nanoparticle based solar cells on flexible glass substrates, *Thin Solid Films* 642 (2017) 110–116, <https://doi.org/10.1016/j.tsf.2017.09.009>.
- J. Li, H. Shen, H. Shang, Y. Li, W. Wu, Performance improvement of flexible CZTSSe thin film solar cell by adding a Ge buffer layer, *Mater. Lett.* 190 (2017) 188–190, <https://doi.org/10.1016/j.matlet.2016.12.106>.
- Y. Zhang, Q. Ye, J. Liu, H. Chen, X. He, C. Liao, J. Han, H. Wang, J. Mei, W. Lau, Earth-abundant and low-cost CZTS solar cell on flexible molybdenum foil, *RSC Adv.* 4 (2014) 23666–23669, <https://doi.org/10.1039/C4RA02064B>.
- Q. Yan, S. Cheng, H. Li, X. Yu, J. Fu, Q. Tian, H. Jia, S. Wu, High flexible $\text{Cu}_2\text{ZnSn}(\text{S,Se})_4$ solar cells by green solution-process, *Sol. Energy* 177 (2019) 508–516, <https://doi.org/10.1016/j.solener.2018.11.030>.
- E. Jo, M.G. Gang, H. Shim, M.P. Suryawanshi, U.V. Ghorpade, J.H. Kim, 8% efficiency $\text{Cu}_2\text{ZnSn}(\text{S,Se})_4$ (CZTSSe) thin film solar cells on flexible and lightweight molybdenum foil substrates, *ACS Appl. Mater. Interfaces* 11 (2019) 23118–23124, <https://doi.org/10.1021/acsami.9b03195>.
- K.-J. Yang, S. Kim, S.-Y. Kim, K. Ahn, D.-H. Son, S.-H. Kim, S.-J. Lee, Y.-I. Kim, S.-N. Park, S.-J. Sung, D.-H. Kim, T. Enkhbat, J. Kim, C.-W. Jeon, J.-K. Kang, Flexible $\text{Cu}_2\text{ZnSn}(\text{S,Se})_4$ solar cells with over 10% efficiency and methods of enlarging the cell area, *Nat. Commun.* 10 (2019) 2959, <https://doi.org/10.1038/s41467-019-10890-x>.
- B.T. Gershon, Y.S. Lee, R. Mankad, O. Gunawan, T. Gokmen, D. Bishop, B. McCandless, S. Guha, The impact of sodium on the sub-bandgap states in CZTSe and CZTS, *Appl. Phys. Lett.* 106 (2015) 123905, <https://doi.org/10.1063/1.4916635>.
- W.M.H. Oo, J.L. Johnson, A. Bhatia, E.A. Lund, M.M. Nowell, M.A. Scarpulla, Grain size and texture of $\text{Cu}_2\text{ZnSnS}_4$ thin films synthesized by cosputtering binary sulfides and annealing: effects of processing conditions and sodium, *J. Electron. Mater.* 40 (2011) 2214–2221, <https://doi.org/10.1007/s11664-011-1729-3>.
- T. Prabhakar, N. Jampana, Effect of sodium diffusion on the structural and electrical properties of $\text{Cu}_2\text{ZnSnS}_4$ thin films, *Sol. Energy Mater. Sol. Cells* 95 (2011) 1001–1004, <https://doi.org/10.1016/j.solmat.2010.12.012>.
- J.V. Li, D. Kuciauskas, M.R. Young, I.L. Repins, Effects of sodium incorporation in Co-evaporated $\text{Cu}_2\text{ZnSnSe}_4$ thin-film solar cells, *Appl. Phys. Lett.* 102 (2013) 163905.
- C.M. Sutter-Fella, J.A. Stückerberger, H. Hagendorfer, F. La Mattina, L. Kranz, S. Nishiwaki, A.R. Uhl, Y.E. Romanyuk, A.N. Tiwari, Sodium assisted sintering of chalcogenides and its application to solution processed $\text{Cu}_2\text{ZnSn}(\text{S,Se})_4$ thin film solar cells, *Chem. Mater.* 26 (2014) 1420–1425, <https://doi.org/10.1063/1.4802972>, doi.org/10.1021/cm403504u.
- G. Rey, F. Babbe, T.P. Weiss, H. Elanzery, M. Melchiorre, N. Valle, B. El Adib, S. Siebentritt, Post-deposition treatment of $\text{Cu}_2\text{ZnSnSe}_4$ with alkalis, *Thin Solid Films* 633 (2017) 162–165, <https://doi.org/10.1016/j.tsf.2016.11.021>.
- K.-J. Yang, S. Kim, J.-H. Sim, D.-H. Son, D.-H. Kim, J. Kim, W. Jo, H. Yoo, J.H. Kim, J.-K. Kang, The alterations of carrier separation in kesterite solar cells, *Nanomater. Energy* 52 (2018) 38–53, <https://doi.org/10.1016/j.nanoen.2018.07.039>.
- M. Kumar, A. Dubey, N. Adhikari, S. Venkatesan, Q. Qiao, Strategic review of secondary phases, defects and defect-complexes in kesterite CZTS–Se solar cells, *Energy Environ. Sci.* 8 (2015) 3134–3159, <https://doi.org/10.1039/C5EE02153G>.
- T. Gershon, B. Shin, N. Bojarczuk, M. Hopstaken, D.B. Mitzi, S. Guha, The role of sodium as a surfactant and suppressor of non-radiative recombination at internal surfaces in $\text{Cu}_2\text{ZnSnS}_4$, *Adv. Energy Mater.* 5 (2015) 1400849, <https://doi.org/10.1002/aenm.201400849>.
- O.P. Singh, K.S. Gour, R. Parmar, V.N. Singh, Sodium induced grain growth, defect passivation and enhancement in the photovoltaic properties of $\text{Cu}_2\text{ZnSnS}_4$ thin film solar cell, *Mater. Chem. Phys.* 177 (2016) 293–298, <https://doi.org/10.1016/j.matchemphys.2016.04.030>.
- T. Maeda, A. Kawabata, T. Wada, First-principles study on alkali-metal effect of Li, Na, and K in $\text{Cu}_2\text{ZnSnS}_4$ and $\text{Cu}_2\text{ZnSnSe}_4$, *Phys. Status Solidi C* 12 (2015) 631–637, <https://doi.org/10.1002/pssc.201400345>.
- Y.-R. Lin, V. Tunuguntla, S.-Y. Wei, W.-C. Chen, D. Wong, C.-H. Lai, L.-K. Liu, L.-C. Chen, K.-H. Chen, Bifacial sodium-incorporated treatments: tailoring deep traps and enhancing carrier transport properties in $\text{Cu}_2\text{ZnSnS}_4$ solar cells, *Nanomater. Energy* 16 (2015) 438–445, <https://doi.org/10.1016/j.nanoen.2015.07.022>.
- J.-H. Min, W.-L. Jeong, K. Kim, J.-S. Lee, K.-P. Kim, J. Kim, M.G. Gang, C.W. Hong, J.H. Kim, D.-S. Lee, Flexible high-efficiency CZTSSe solar cells on diverse flexible substrates via an adhesive-bonding transfer method, *ACS Appl. Mater. Interfaces* 12 (2020) 8189–8197, <https://doi.org/10.1021/acsami.9b19909>.
- Q. Tian, X. Xu, L. Han, M. Tang, R. Zou, Z. Chen, M. Yu, J. Yang, J. Hu, Hydrophilic $\text{Cu}_2\text{ZnSnS}_4$ nanocrystals for printing flexible, low-cost and environmentally friendly solar cells, *CrystEngComm* 14 (2012) 3847–3850, <https://doi.org/10.1039/C2CE06552E>.
- K. Sun, F. Liu, J. Huang, C. Yan, N. Song, H. Sun, C. Xue, Y. Zhang, A. Pu, Y. Shen, J.A. Stride, M. Green, X. Hao, Flexible kesterite $\text{Cu}_2\text{ZnSnS}_4$ solar cells with sodium-doped molybdenum back contacts on stainless steel substrates, *Sol. Energy Mater. Sol. Cells* 182 (2018) 14–20, <https://doi.org/10.1016/j.solmat.2018.02.036>.
- K. Sun, F. Liu, C. Yan, F. Zhou, J. Huang, Y. Shen, R. Liu, X. Hao, Influence of sodium incorporation on kesterite $\text{Cu}_2\text{ZnSnS}_4$ solar cells fabricated on stainless steel substrates, *Sol. Energy Mater. Sol. Cells* 157 (2016) 565–571, <https://doi.org/10.1016/j.solmat.2016.07.036>.
- S. López-Marino, Y. Sánchez, M. Espíndola-Rodríguez, X. Alcobé, H. Xie, M. Neuschitzer, I. Becerril, S. Giraldo, M. Dimitrievska, M. Placidi, L. Fourdrinier, V. Izquierdo-Roca, A. Pérez-Rodríguez, E. Saucedo, Alkali doping strategies for

- flexible and light-weight $\text{Cu}_2\text{ZnSnSe}_4$ solar cells, *J. Mater. Chem. A* 4 (2016) 1895–1907, <https://doi.org/10.1039/C5TA09640E>.
- [36] S. López-Marino, M. Neuschitzer, Y. Sánchez, A. Fairbrother, M. Espindola-Rodríguez, J. López-García, M. Placidi, L. Calvo-Barrio, A. Pérez-Rodríguez, E. Saucedo, Earth-abundant absorber based solar cells onto low weight stainless steel substrate, *Sol. Energy Mater. Sol. Cells* 130 (2014) 347–353, <https://doi.org/10.1016/j.solmat.2014.07.030>.
- [37] Z. Zhou, Y. Wang, D. Xu, Y. Zhang, Fabrication of $\text{Cu}_2\text{ZnSnS}_4$ screen printed layers for solar cells, *Sol. Energy Mater. Sol. Cells* 94 (2010) 2042–2045, <https://doi.org/10.1016/j.solmat.2010.06.010>.
- [38] W.-L. Jeong, K.-P. Kim, J. Kim, H.K. Park, J.-H. Min, J.-S. Lee, S.-H. Mun, S.-T. Kim, J.-H. Jang, W. Jo, D.-S. Lee, Impact of Na doping on the carrier transport path in polycrystalline flexible $\text{Cu}_2\text{ZnSn(S,Se)}_4$ solar cells, *Adv. Sci.* 7 (2020) 1903085, <https://doi.org/10.1002/advs.201903085>.
- [39] G.Y. Kim, J. Kim, W. Jo, K.D. Lee, J.Y. Kim, T.T.T. Nguyen, S. Yoon, Effects of Cu_{2-x}S phase removal on surface potential of $\text{Cu}_2\text{ZnSnS}_4$ thin-films grown by electroplating, *Curr. Appl. Phys.* 14 (2014) 1665–1668, <https://doi.org/10.1016/j.cap.2014.09.009>.
- [40] N. Benhaddou, S. Aazou, Y. Sánchez, J. Andrade-Arvizu, I. Becerril-Romero, M. Guc, S. Giraldo, V. Izquierdo-Roca, E. Saucedo, Z. Sekkat, Investigation on limiting factors affecting $\text{Cu}_2\text{ZnGeSe}_4$ efficiency: effect of annealing conditions and surface treatment, *Sol. Energy Mater. Sol. Cells* 216 (2020) 110701, <https://doi.org/10.1016/j.solmat.2020.110701>.
- [41] D. Colombara, H. Elanzeery, N. Nicoara, D. Sharma, M. Claro, T. Schwarz, A. Koprek, M.H. Wolter, M. Melchiorre, M. Sood, N. Valle, O. Bondarchuk, F. Babbe, C. Spindler, O. Cococar-Miredin, D. Raabe, P.J. Dale, S. Sadewasser, S. Siebentritt, Chemical instability at chalcogenide surfaces impacts chalcopyrite devices well beyond the surface, *Nat. Commun.* 11 (2020) 3634, <https://www.nature.com/articles/s41467-020-17434-8>.
- [42] J.Y.W. Seto, The electrical properties of polycrystalline silicon films, *J. Appl. Phys.* 46 (1975) 5247, <https://doi.org/10.1063/1.321593>.
- [43] J.B. Li, V. Chawla, B.M. Clemens, Investigating the role of grain boundaries in CZTS and CZTSSe thin film solar cells with scanning probe microscopy, *Adv. Mater.* 24 (2012) 720–723, <https://doi.org/10.1002/adma.201103470>.
- [44] H. Monig, Y. Smith, R. Caballero, C.A. Kaufmann, I. Lauermann, M. Lux-Steiner, S. Sadewasser, Direct evidence for a reduced density of deep level defects at grain boundaries of Cu(In,Ga)Se_2 thin films, *Phys. Rev. Lett.* 105 (2010) 116802, <https://doi.org/10.1103/PhysRevLett.105.116802>.
- [45] C.S. Jiang, R. Noufi, K. Ramanathan, J.A. AbuShama, H.R. Moutinho, M.M. Al-Jassim, Does the local built-in potential on grain boundaries of Cu(In,Ga)Se_2 thin films benefit photovoltaic performance of the device? *Appl. Phys. Lett.* 85 (2004) 2625–2627, <https://doi.org/10.1063/1.1793346>.
- [46] C.S. Jiang, R. Noufi, J.A. AbuShama, K. Ramanathan, H.R. Moutinho, J. Pankow, M.M. Al-Jassim, Local built-in potential on grain boundary of Cu(In,Ga)Se_2 thin films, *Appl. Phys. Lett.* 84 (2004) 3477–3479, <https://doi.org/10.1063/1.1737796>.
- [47] Y. Yan, C.S. Jiang, R. Noufi, S.H. Wei, H.R. Moutinho, M.M. Al-Jassim, Electrically benign behavior of grain boundaries in polycrystalline CuInSe_2 films, *Phys. Rev. Lett.* 99 (2007) 235504, <https://doi.org/10.1103/PhysRevLett.99.235504>.
- [48] A. Nagaoka, H. Miyake, T. Taniyama, K. Kakimoto, Y. Nose, M.A. Scarpulla, K. Yoshino, Effects of sodium on electrical properties in $\text{Cu}_2\text{ZnSnS}_4$ single crystal, *Appl. Phys. Lett.* 104 (2014) 152101, <https://doi.org/10.1063/1.4871208>.
- [49] J. Kim, G.Y. Kim, T.T.T. Nguyen, S. Yoon, Y.-K. Kim, S.-Y. Lee, M. Kim, D.-H. Cho, Y.-D. Chung, J.-H. Lee, M.-J. Seong, W. Jo, Sodium-assisted passivation of grain boundaries and defects in $\text{Cu}_2\text{ZnSnSe}_4$ thin films, *Phys. Chem. Chem. Phys.* 22 (2020) 7597–7605, <https://doi.org/10.1039/C9CP06537G>.
- [50] G.Y. Kim, D.-H. Son, T.T.T. Nguyen, S. Yoon, M. Kwon, C.-W. Jeon, D.-H. Kim, J.-K. Kang, W. Jo, Enhancement of photo-conversion efficiency in $\text{Cu}_2\text{ZnSn(S,Se)}_4$ thin-film solar cells by control of ZnS precursor-layer thickness, *Prog. Photovolt.* 24 (2015) 292–306, <https://doi.org/10.1002/ppp.2693>.
- [51] A. Polizzotti, I.L. Repins, R. Noufi, S.-H. Wei, D.B. Mitzi, The state and future prospects of kesterite photovoltaics, *Energy Environ. Sci.* 6 (2013) 3171–3182, <https://doi.org/10.1039/C3EE41781F>.
- [52] J.-S. Park, S. Kim, Z. Xie, A. Walsh, Point defect engineering in thin-film solar cells, *Nat. Rev. Mater.* 3 (2018) 194, <https://doi.org/10.1038/s41578-018-0026-7>.
- [53] W.-J. Yin, Y. Wu, S.-H. Wei, R. Noufi, M.M. Al-Jassim, Y. Yan, Engineering grain boundaries in $\text{Cu}_2\text{ZnSnSe}_4$ for better cell performance: a first-principle study, *Adv. Energy Mater.* 4 (2014) 1300712, <https://doi.org/10.1002/aenm.201300712>.
- [54] Z. Su, K. Sun, Z. Han, H. Cui, F. Liu, Y. Lai, J. Li, X. Hao, Y. Liu, M.A. Green, Fabrication of $\text{Cu}_2\text{ZnSnS}_4$ solar cells with 5.1% efficiency via thermal decomposition and reaction using a non-toxic sol-gel route, *J. Mater. Chem.* 2 (2014) 500–509, <https://doi.org/10.1039/C3TA13533K>.
- [55] C.-Y. Liu, Z.-M. Li, H.-Y. Gu, S.-Y. Chen, H. Xiang, X.-G. Gong, Sodium passivation of the grain boundaries in CuInSe_2 and $\text{Cu}_2\text{ZnSnS}_4$ for high-efficiency solar cells, *Adv. Energy Mater.* 7 (2017) 1601457, <https://doi.org/10.1002/aenm.201601457>.
- [56] Y. Sun, H. Guo, P. Qiu, S. Zhang, S. Wang, L. Wu, J. Ao, Y. Zhang, Na-doping-induced modification of the $\text{Cu}_2\text{ZnSn(S,Se)}/\text{CdS}$ heterojunction towards efficient solar cells, *J. Energy Chem.* (2020), <https://doi.org/10.1016/j.jechem.2020.09.007> (in press).
- [57] M. Han, X. Zhang, Z. Zeng, An investigation of Na-related defects in $\text{Cu}_2\text{ZnSnSe}_4$, *Phys. Chem. Chem. Phys.* 19 (2017) 17799–17804, <https://doi.org/10.1039/c7cp02192e>.
- [58] X. Sun, X. Wang, P. Wang, B. Sheng, M. Li, J. Su, J. Zhang, F. Liu, X. Rong, F. Xu, X. Yang, Z. Qin, W. Ge, B. Shen, Identifying a doping type of semiconductor nanowires by photoassisted kelvin probe force microscopy as exemplified for GaN nanowires, *Opt. Mater. Express* 7 (2017) 904–912, <https://doi.org/10.1364/OME.7.000904>.
- [59] M. Igalson, A. Urbaniak, P. Zabierowski, H.A. Maksoud, M. Buffiere, N. Barreau, S. Spiering, Red-blue effect in Cu(In,Ga)Se_2 -based devices revisited, *Thin Solid Films* 535 (2013) 302–306, <https://doi.org/10.1016/j.tsf.2012.11.040>.
- [60] A.O. Pudov, J.R. Sites, M.A. Contreras, T. Nakada, H.W. Schock, CIGS J-V distortion in the absence of blue photons, *Thin Solid Films* 480–481 (2005) 273–278, <https://doi.org/10.1016/j.tsf.2004.11.099>.
- [61] Y. Cho, J. Hwang, I. Jeong, J. Gwak, J.H. Yun, K. Kim, W. Jo, Photon-induced defects and dynamics of photogenerated carriers in Cu(In,Ga)Se_2 thin film solar cells, *Sol. Energy Mater. Sol. Cells* 220 (2021) 110860, <https://doi.org/10.1016/j.solmat.2020.110860>.
- [62] H.C. Gatos, J. Lagowski, Surface photovoltage spectroscopy—a new approach to the study of high-gap semiconductor surfaces, *J. Vac. Sci. Technol.* 10 (1973) 130–135, <https://doi.org/10.1116/1.1317922>.
- [63] L. Kronik, Y. Shapira, Surface photovoltage phenomena: theory, experiment, and applications, *Surf. Sci. Rep.* 37 (1999) 1–206, [https://doi.org/10.1016/S0167-5729\(99\)00002-3](https://doi.org/10.1016/S0167-5729(99)00002-3).
- [64] S. Tajima, R. Asahi, D. Isheim, D.N. Seidman, T. Itoh, K. Ohishi, Sodium distribution in solar-grade $\text{Cu}_2\text{ZnSnS}_4$ layers using atom-probe tomographic technique, *Jpn. J. Appl. Phys.* 54 (2015) 112302, <https://doi.org/10.7567/JJAP.54.112302>.
- [65] K.-J. Yang, J.-H. Sim, B. Jeon, D.-H. Son, D.-H. Kim, S.-J. Sung, D.-K. Hwang, S. Song, D.B. Khadka, J. Kim, J.-K. Kang, Effects of Na and MoS_2 on $\text{Cu}_2\text{ZnSnS}_4$ thin-film solar cell, *Prog. Photovolt.* 23 (2015) 862–873, <https://doi.org/10.1002/ppp.2500>.
- [66] C. Heske, R. Fink, E. Umbach, W. Riedl, F. Karg, Na-induced effects on the electronic structure and composition of Cu(In,Ga)Se_2 thin-film surfaces, *Appl. Phys. Lett.* 68 (1996) 3431–3433, <https://doi.org/10.1063/1.115783>.
- [67] K. Momma, F. Izumi, VESTA 3 for three-dimensional visualization of crystal, volumetric and morphology data, *J. Appl. Crystallogr.* 44 (2011) 1272–1276, <https://doi.org/10.1107/S00218898110038970>.
- [68] M. Leibovitch, L. Kronik, E. Fefer, L. Burstein, V. Korobov, Y. Shapira, Surface photovoltage spectroscopy of thin films, *J. Appl. Phys.* 79 (1996) 8549–8556, <https://doi.org/10.1063/1.362535>.
- [69] Z. Zhang, J.T. Yates Jr., Band bending in semiconductors: chemical and physical consequences at surfaces and interfaces, *Chem. Rev.* 112 (2012) 5520–5551, <https://doi.org/10.1021/cr3000626>.
- [70] L. Kronik, Y. Shapira, Surface photovoltage spectroscopy of semiconductor structures: at the crossroads of physics, chemistry and electrical engineering, *Surf. Interface Anal.* 31 (2001) 954–965, <https://doi.org/10.1002/sia.1132>.
- [71] M.A. Deeb, J. Ledig, J. Wei, X. Wang, H.-H. Wehmann, A. Waag, Photo-assisted Kelvin probe force microscopy investigation of three dimensional GaN structures with various crystal facets, doping types, and wavelengths of illumination, *J. Appl. Phys.* 122 (2017), 085307, <https://doi.org/10.1063/1.5000137>.
- [72] D. Hironiwa, J. Chantana, N. Sakai, T. Kato, H. Sugimoto, T. Minemoto, Application of multi-buffer layer of $(\text{Zn,Mg})\text{O}/\text{CdS}$ in $\text{Cu}_2\text{ZnSn(S,Se)}_4$ solar cells, *Curr. Appl. Phys.* 15 (2015) 383–388, <https://doi.org/10.1016/j.cap.2015.01.011>.
- [73] S. Schorr, G. Gurieva, M. Guc, M. Dimitrievska, A. Pérez-Rodríguez, V. Izquierdo-Roca, C.S. Schnorr, J. Kim, W. Jo, J.M. Merino, Point defects, compositional fluctuations, and secondary phases in non-stoichiometric kesterites, *J. Phys. Energy* 2 (2020), 012002, <https://doi.org/10.1088/2515-7655/ab4a25>.
- [74] H.-S. Duan, W. Yang, B. Bob, C.-J. Hsu, B. Lei, Y. Yang, The role of sulfur in solution-processed $\text{Cu}_2\text{ZnSn(S,Se)}_4$ and its effect on defect properties, *Adv. Funct. Mater.* 23 (2013) 1466–1471, <https://doi.org/10.1002/adfm.201201732>.
- [75] C.J. Hages, N.J. Carter, R. Agrawal, T. Unold, Generalized current-voltage analysis and efficiency limitations in non-ideal solar cells: case of $\text{Cu}_2\text{ZnSn(S}_x\text{Se}_{1-x})_4$ and $\text{Cu}_2\text{Zn(Sn}_y\text{Ge}_{1-y})(\text{S}_x\text{Se}_{1-x})_4$, *J. Appl. Phys.* 115 (2014) 234504, <https://doi.org/10.1063/1.4882119>.